AGU100 ADVANCING EARTH AND SPACE SCIENCE

Geophysical Research Letters

RESEARCH LETTER
10.1029/2018GL077905

Key Points:
- Bistatic radar observations of reflection power from CYGNSS are compared to SMAP soil moisture retrievals
- Changes in CYGNSS reflectivity and changes in soil moisture exhibit strong linear relationships, with spatially varying slopes
- The unbiased root-mean-square difference between CYGNSS and SMAP is 0.045 cm^3/cm^3 and is similar between CYGNSS and in situ observations

Supporting Information:
- Supporting Information S1
- Figure S1
- Figure S2
- Figure S3
- Figure S4

Correspondence to:
C. C. Chew,
clarac@ucar.edu;
clara.c.chew@gmail.com

Citation:
Chew, C. C., & Small, E. E. (2018). Soil moisture sensing using spaceborne GNSS reflections: Comparison of CYGNSS reflectivity to SMAP soil moisture. *Geophysical Research Letters*, *45*, 4049–4057. https://doi.org/10.1029/2018GL077905

Received 13 MAR 2018
Accepted 5 APR 2018
Accepted article online 19 APR 2018
Published online 5 MAY 2018

Soil Moisture Sensing Using Spaceborne GNSS Reflections: Comparison of CYGNSS Reflectivity to SMAP Soil Moisture

C. C. Chew[1] **and E. E. Small**[2]

[1]University Corporation for Atmospheric Research, Boulder, CO, USA, [2]Department of Geological Sciences, University of Colorado Boulder, Boulder, CO, USA

Abstract This paper quantifies the relationship between forward scattered L-band Global Navigation Satellite System (GNSS) signals, recorded by the Cyclone Global Navigation Satellite System (CYGNSS) constellation and Soil Moisture Active Passive (SMAP) soil moisture (SM). Although designed for tropical ocean surface wind sensing, the CYGNSS receivers also record GNSS reflections over land. The CYGNSS observations of reflection power are compared to SMAP SM between March 2017 and February 2018. A strong, positive linear relationship exists between changes in CYGNSS reflectivity and changes in SMAP SM, but not between the absolute magnitudes of the two observations. The sensitivity of CYGNSS reflectivity to SM varies spatially and can be used to convert reflectivity to estimates of SM. The unbiased root-mean-square difference between daily averaged CYGNSS-derived SM and SMAP SM is 0.045 cm^3/cm^3 and is similarly low between CYGNSS and in situ SM. These results show that CYGNSS, and future GNSS reflection missions, could provide global SM observations.

Plain Language Summary Satellite remote sensing of near-surface soil moisture is needed to improve weather forecasts and climate models. This is normally accomplished using one of two types of instruments: a radiometer, which provides data every 2–3 days but with a spatial resolution of ~40 km, or a monostatic radar, which provides data once every few weeks, but with subkilometer spatial resolution. These instruments are expensive—National Aeronautics and Space Administration's Soil Moisture Active Passive (SMAP) mission cost upward of a billion dollars. Here we present evidence that there is a third option for soil moisture remote sensing, which is hundreds of millions of dollars less expensive than current instruments and provides approximately daily data with few kilometers spatial sensitivity. This third method uses transmitted Global Navigation Satellite System (GNSS) signals, which are recorded by the Cyclone GNSS (CYGNSS) constellation of eight satellites. We show that these data are sensitive to soil moisture changes across a broad range of environments and through time. There are strong linear relationships between CYGNSS data and SMAP data, as well as ground-based observations. The data are currently available and could be used to infill the 2- to 3-day SMAP time series.

1. Introduction

Soil moisture (SM) plays an important role in the climate system, affecting atmospheric conditions, hydrologic processes, and vegetation state (Entekhabi et al., 1996; Koster et al., 2004; Rodriguez-Iturbe, 2000). Satellite-based monitoring of SM is needed for improved weather and climate forecasts and hydrologic modeling. Two L-band passive microwave radiometers currently provide global measurements of SM: the Soil Moisture and Ocean Salinity and Soil Moisture Active Passive (SMAP) missions (Entekhabi et al., 2010; Kerr et al., 2012). Both provide SM retrievals for the top 5 cm of the soil column, with spatial resolution of ~40 km and revisit time of 2–3 days. Surface SM is also measured globally with monostatic radar: a single antenna transmits and then receives a backscattered signal, for example, using Advanced Scatterometer (Naeimi et al., 2009) or Sentinel-1 data (Geudtner & Torres, 2012), both at C-band. Passive and active measurements are complementary; data assimilation that incorporates both types of measurements provides the best results (Draper et al., 2012; Lievens et al., 2017).

A third approach to measure SM with microwave remote sensing is with bistatic radar: the signal is transmitted by an antenna from one platform, scatters in the forward direction off the Earth's surface, and is received by a second antenna on a different platform. Like other microwave signals, bistatic radar signals are affected by SM, as well as overlying vegetation canopies, surface roughness, and topography

(Guerriero et al., 2013; Pierdicca et al., 2014). Signals from Global Navigation Satellite System (GNSS) constellations can be used as the signal source, with the surface-reflected signals recorded by a specialized receiver. This approach is referred to as GNSS-reflectometry (GNSS-R) and has been used to monitor both ocean and land characteristics (Cardellach et al., 2011; Clarizia et al., 2009; Foti et al., 2015; Katzberg et al., 2006; Komjathy et al., 2000; Larson et al., 2008; Masters et al., 2000; Valencia et al., 2014). GNSS-R has been used specifically to monitor SM (Egido et al., 2014; Larson et al., 2008; Masters, 2004; Rodriguez-Alvarez et al., 2011; Small et al., 2016). However, as with nearly all other previous GNSS-R studies, the receivers used in these studies were mounted on towers or planes.

With satellite receivers, GNSS-R has the potential to provide a new approach to monitor SM at the global scale that complements existing passive and active radar systems. The Cyclone GNSS (CYGNSS) mission, a constellation of eight satellites carrying GNSS-R receivers, was launched in December 2016 (Ruf et al., 2016). CYGNSS was designed to observe ocean winds in the tropics, but reflections are also measured from the land surface, and these data could be used to retrieve SM. CYGNSS and similar GNSS-R instruments have several characteristics that make them attractive for SM remote sensing. First, GNSS signals are at L-band, which is optimal for SM remote sensing due to the increased ability to penetrate vegetation relative to shorter wavelengths (De Roo et al., 2001). Second, a constellation of receivers shortens revisit time compared to a single satellite. Third, transmitted GNSS signals exist for other purposes, reducing the cost of the complete sensing system.

Previously, it has been shown that spaceborne GNSS reflections are sensitive to land surface conditions (Camps et al., 2016; Chew et al., 2016). These studies used data from a reflectometry instrument on board TechDemoSat-1 (TDS-1), which was similar to instruments on CYGNSS. However, the data volume collected by TDS-1 was several orders of magnitude less than that collected by CYGNSS. Accordingly, the revisit time of TDS-1 was $>$6 months while that from CYGNSS is ~1 day. Thus, the previous TDS-1 studies were nearly exclusively an evaluation of the spatial correspondence between the GNSS signal and SM at a single instant in time. Time series analyses were not possible. Here we demonstrate that the temporal fluctuations of the CYGNSS signal have a much stronger correlation with SM than the absolute magnitude of reflectivity that could be measured by TDS-1. The CYGNSS constellation allows for the first comprehensive test of where and under what circumstances do GNSS reflections respond to fluctuations in SM on timescales of days to seasons.

Here we compare CYGNSS observations to SM retrievals from the SMAP L-band radiometer. Satellite intercomparisons, such as that completed here, are commonly used to quantify similarities and differences between various data sources (e.g., Brocca et al., 2011; Burgin et al., 2017; Rudiger et al., 2009; Su et al., 2013). Our comparison to SMAP allows for a rapid evaluation of CYGNSS over many parts of the Earth's land surface, including a wide range of vegetation and roughness conditions. We also compare CYGNSS to observations from four in situ SM monitoring sites.

The goal of this paper is to demonstrate the possibility of using spaceborne GNSS reflections to observe SM. CYGNSS was not designed for land surface remote sensing and thus is not an ideal SM Sensor. Various aspects of the CYGNSS data collection strategy could be modified to enhance its utility for terrestrial remote sensing. The analysis presented here can help guide these improvements.

2. Data

2.1. SM Data

SMAP collects dual-pol brightness temperature observations from an L-band microwave radiometer, which are then converted into SM. SMAP's native resolution is ~40 km, with SM retrievals posted to a 36-km grid (Entekhabi et al., 2010). We do not compare CYGNSS observations to SMAP in areas that are flagged as "not recommended for retrieval," including flags for high surface water fraction, dense vegetation ($>$5 kg/m^2 vegetation water content), and urban and mountainous areas (O'Neill et al., 2016). SMAP SM is also available on a 9-km grid (Chan et al., 2018). Here we use the Level 3 36-km gridded product, as this increases the number of contemporaneous CYGNSS and SMAP observations by sixteenfold.

2.2. CYGNSS Data

Each of the eight CYGNSS satellites records four GNSS signals at one time. The receivers orbit the tropics, which limits their spatial coverage to latitudes ±37°. The observable of interest, the forward scattered

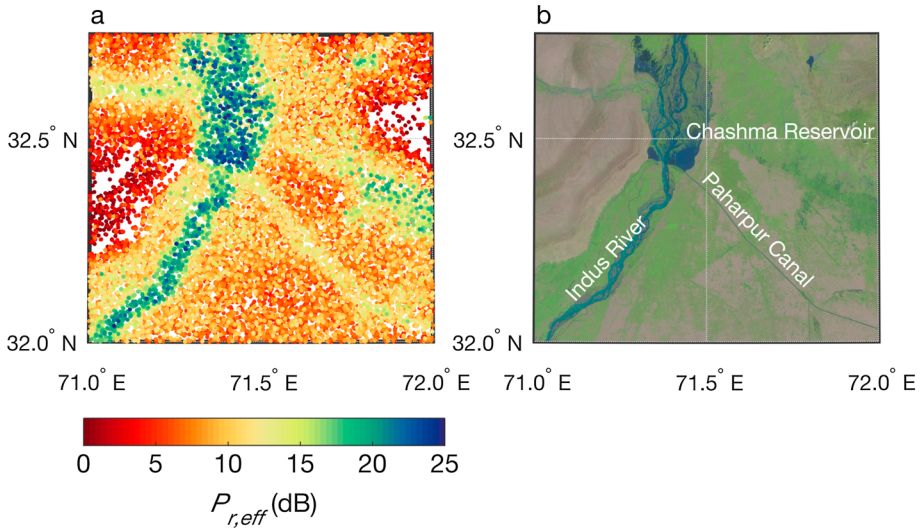

Figure 1. (a) Observations of $P_{r,\mathrm{eff}}$ from Cyclone Global Navigation Satellite System for the time period 18 March 2017 to 17 February 2018, in northern Pakistan. (b) Landsat image from 15 August 2017, for the same region.

signal power, will be denoted as $P_{r,\mathrm{eff}}$ (Chew et al., 2016). The analysis to determine $P_{r,\mathrm{eff}}$ is described in the supporting information. This paper uses CYGNSS data from 18 March 2017 to 17 February 2018.

The dimensions of the sensing footprint that affect each $P_{r,\mathrm{eff}}$ observation have not yet been definitively quantified. The theoretical footprint of a reflected GNSS signal is ~0.5 × 0.5 km, for the case of a smooth surface and a receiver at the altitude of CYGNSS, with slight dependence on the incidence angle (Katzberg & Garrison, 1996). As surface roughness increases, the spatial resolution is degraded. For a very rough surface like the ocean, the spatial resolution is ~25 × 25 km; Ruf et al., 2016). The CYGNSS receivers integrate signals over 1 s to accommodate the weak reflections coming from the rough ocean surface. During this period of time, the receiver travels ~7 km. Thus, the smallest area of ground from which reflections are received is ~7 × 0.5 km (Figure S1).

Comparisons to optical images suggest that $P_{r,\mathrm{eff}}$ is sensitive to land surface features 1 km or smaller. Figure 1 shows observations of $P_{r,\mathrm{eff}}$ along with an optical image for a region in northern Pakistan. Higher $P_{r,\mathrm{eff}}$ is observed over water bodies, and lower $P_{r,\mathrm{eff}}$ is observed in dry desert areas. This is expected because wet surfaces produce stronger reflections than dry surfaces (Chew et al., 2016; Nghiem et al., 2017). Wetter surfaces have higher dielectric constants, which results in higher reflectivity than drier surfaces (Dobson et al., 1985; Egido, 2013; Masters, 2004). The presence of vegetation should result in lower $P_{r,\mathrm{eff}}$ relative to bare surfaces, due to volume scattering within the canopy (Ferrazzoli et al., 2011).

This figure highlights the sensitivity of the CYGNSS observations to small-scale surface features, though the true spatial resolution is still unknown. The Indus River in this location is ~2–3 km across, while the Paharpur Canal is only 200- to 300-m wide. Observations near the canal are over 5 dB higher than observations in the surrounding desert. The sensitivity to fine-scale surface features guides our strategy to compare CYGNSS and SMAP. The ever-changing geometries of the GNSS satellites and CYGNSS satellites result in a quasi-random sampling of the Earth's surface, which is different from the repeatable swath-like sampling of most remote sensing satellites (Figure S1). Given the sensitivity to fine-scale surface features and the pseudorandom sampling of CYGNSS, we upscale CYGNSS observations to the 36-km resolution of SMAP through averaging, described below.

Because of the pseudorandom surface sampling, temporal repeat times are probabilistic. Each day, ~80% of the 36 × 36-km SMAP pixels on the land surface contain at least one CYGNSS specular reflection point (Figure S2). However, the entirety of each pixel is not sampled, only a portion (Figure S1). Mixed pixels with different land cover types will thus result in day-to-day variation in $P_{r,\mathrm{eff}}$ that are due to the difference in sampling locations within a single SMAP pixel. This is one component of uncertainty in the comparison of CYGNSS and SMAP.

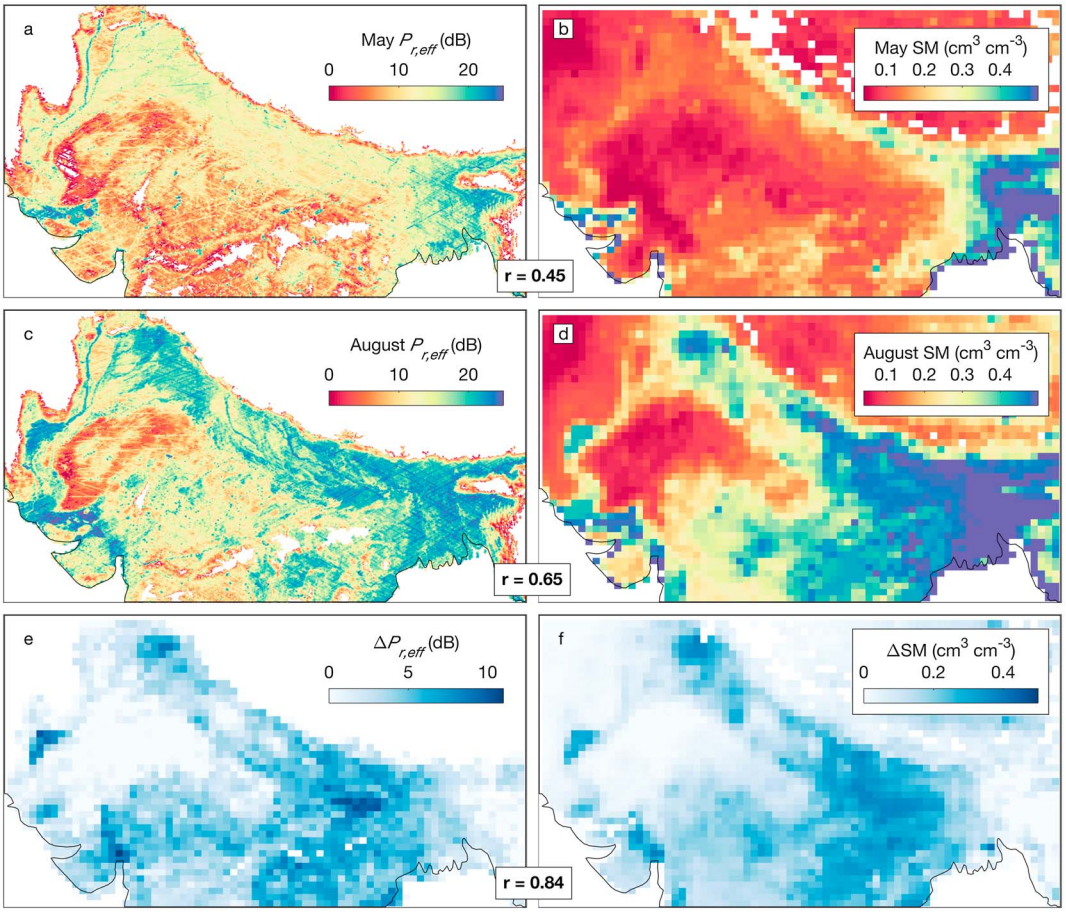

Figure 2. Observations of $P_{r,eff}$ for May (a) and August (c) 2017, in northern India and Pakistan. Also shown is mean soil moisture (SM) for May (b) and August (d) 2017, retrieved by Soil Moisture Active Passive for the same region. (e) Changes in $P_{r,eff}$, gridded to 36 km, between May and August. (f) Changes in SM between May and August. Corresponding brightness temperature observations from Soil Moisture Active Passive are shown in Figure S3.

3. Relationship Between CYGNSS Reflectivity and SMAP SM

3.1. Observations in Northern India and Pakistan

Figure 2 shows $P_{r,eff}$ in northern India and Pakistan for May (Figure 2a) and August (Figure 2c) 2017. These observations are not gridded—shown are all of the observations in both months. Areas with a surface elevation exceeding 600 m have been masked out due to an altitude limitation in the CYGNSS observations. Between May and August, $P_{r,eff}$ increased significantly in several regions. In order to calculate the change in $P_{r,eff}$ between these two time periods, we gridded the data to the SMAP 36-km grid (mean number of CYGNSS observations per grid cell: 140 in May and 291 in August). Overall, $P_{r,eff}$ increased from May to August (Figure 2e), with 5- to 10-dB increases observed in the majority of the region.

Figures 2b and 2d show mean SMAP SM averaged for the same time periods. There is only a moderate spatial correspondence between $P_{r,eff}$ and SMAP SM, in both May and August (r = 0.45 for May and r = 0.65 for August). This is expected because $P_{r,eff}$ is influenced by topography, surface water, and land cover, not just SM. The correlation calculation was completed using the $P_{r,eff}$ observations gridded to the 36-km SMAP scale. The result is very different when we compare the changes between the 2 months. SM increases in many parts of the region (Figure 2f) as a result of summer monsoon rainfall. There is a strong correlation between the May-to-August changes in $P_{r,eff}$ and SMAP SM (r = 0.84). Due to the fact that there is limited correlation between spatial variations in $P_{r,eff}$ and SMAP SM but high correlation between temporal changes in $P_{r,eff}$ and SM, we focus on temporal changes in the observations for the remainder of this analysis.

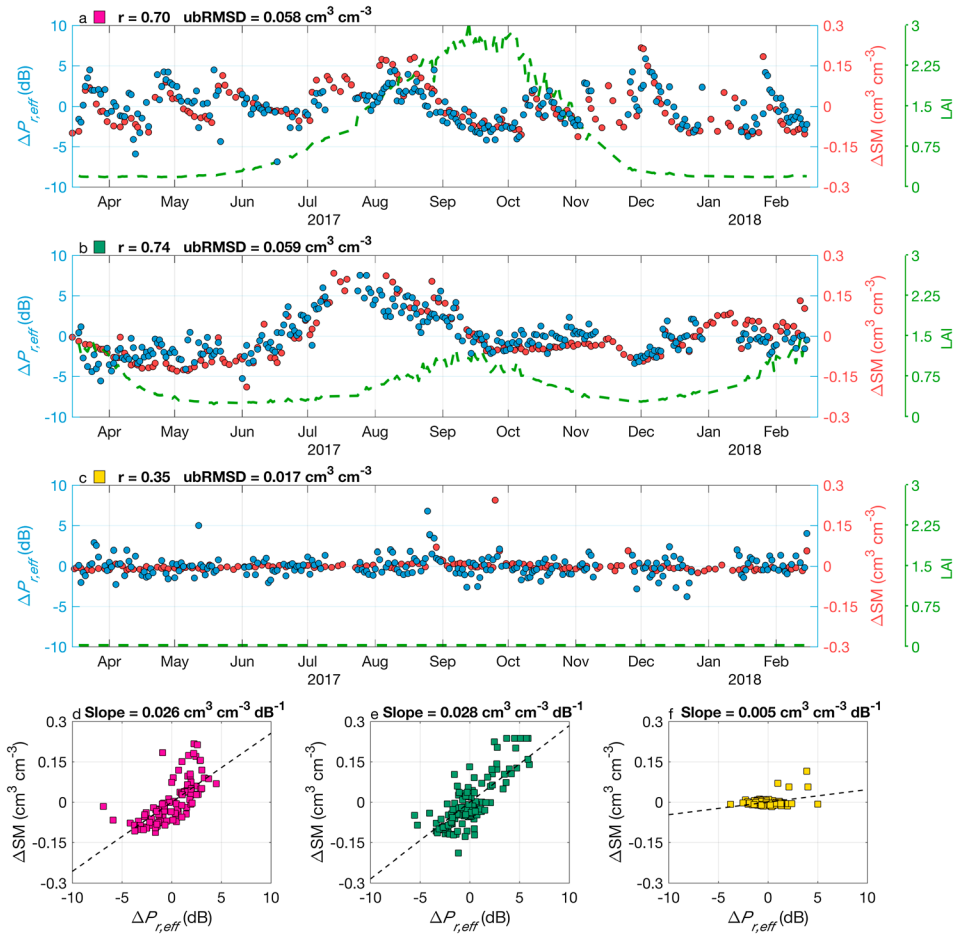

Figure 3. (a–c) Daily averaged time series of $\Delta P_{r,\mathrm{eff}}$, ΔSM, and leaf area index (LAI) for locations indicated by the colored squares on the map in Figure 4. (e and f) The relationship between $\Delta P_{r,\mathrm{eff}}$ and ΔSM for the time series shown in (a)–(c). The best fit linear regression line and slope of the best fit line are also shown. SM = soil moisture; ubRMSD = unbiased root-mean-square difference.

3.2. Temporal Changes in $P_{r,\mathrm{eff}}$ and SMAP SM

We now describe the relationship between temporal changes in $P_{r,\mathrm{eff}}$ and SMAP SM for each 36-km grid cell. We exclude cells that are regularly flagged as producing poor quality SM retrievals or with an altitude greater than 600 m. For each grid cell, we calculate temporal deviations of daily averaged $P_{r,\mathrm{eff}}$ with respect to mean value for that grid cell for the entire time period of interest (18 March 2017 to 17 February 2018), referred to as $\Delta P_{r,\mathrm{eff}}$. We calculate ΔSM the same way: differences from the mean SM value for the entire period of observation for each grid cell are calculated. We then compare $\Delta P_{r,\mathrm{eff}}$ to ΔSM for each grid cell and calculate the correlation coefficient and slope of the linear regression. The slope of the linear regression between $\Delta P_{r,\mathrm{eff}}$ and ΔSM represents the sensitivity of $P_{r,\mathrm{eff}}$ to SM: higher slopes indicating a lower sensitivity of $P_{r,\mathrm{eff}}$ to SM and smaller slopes indicating a higher sensitivity to SM.

Figure 3 shows time series of $\Delta P_{r,\mathrm{eff}}$ and ΔSM for three locations in the tropics, along with corresponding time series of leaf area index (LAI). These locations were chosen because they represent a range of environments and regions in terms of SM variability and vegetation density. Figure 3a shows data from southern Australia where maximum LAI is 3.0. At this site, SM varies on timescales of weeks to months. Fluctuations in $\Delta P_{r,\mathrm{eff}}$ are similar to ΔSM ($r = 0.7$) across the full range of LAI. SM at a location in northern India varies on a much longer timescale—there is a 3-month period with high SM associated with the Indian monsoon (Figure 3b). Again, fluctuations in $\Delta P_{r,\mathrm{eff}}$ mimic the observed variations in SM ($r = 0.74$). Figure 3c shows a desert site in northern Africa with little or no vegetation (LAI = 0). SMAP shows little or no variations in SM. The $\Delta P_{r,\mathrm{eff}}$ record is

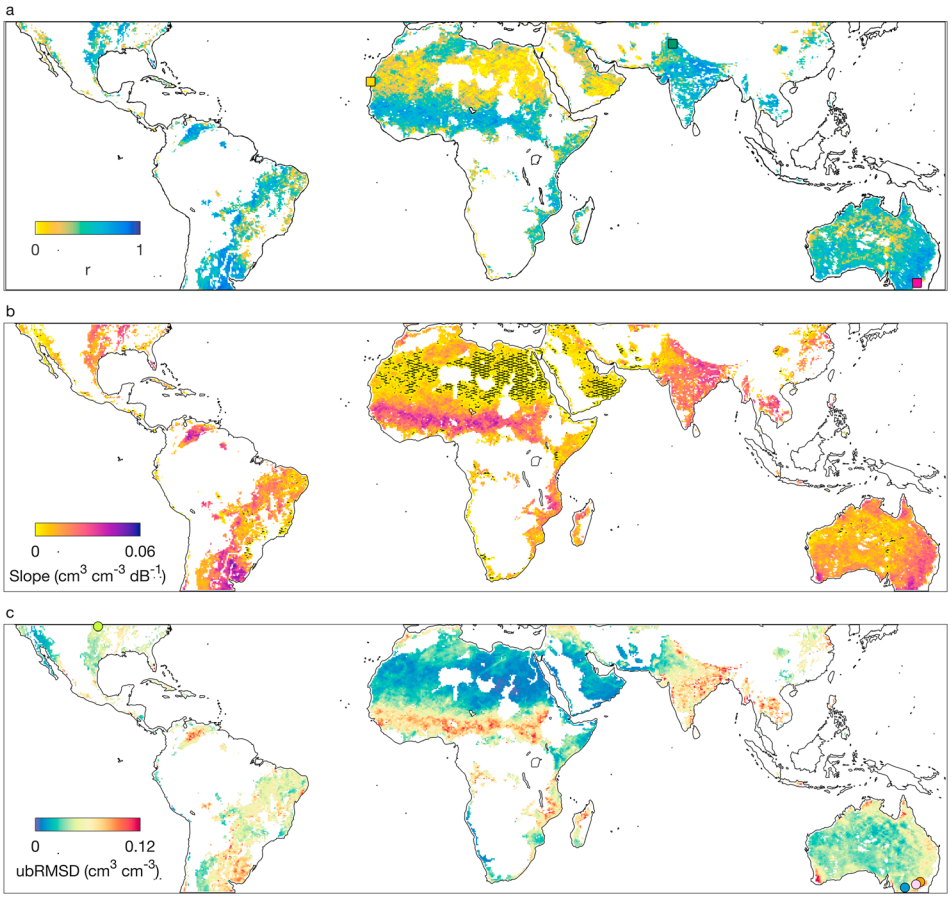

Figure 4. (a) Correlation coefficients between daily averaged observations of $\Delta P_{r,\mathrm{eff}}$ and ΔSM. Colored squares are locations shown by the time series in Figure 3. (b) The slope of the best fit linear regression between $\Delta P_{r,\mathrm{eff}}$ and ΔSM. Hatch-marked areas are regions where the slope is likely not representative of true sensitivity (regions where $r < 0.2$). (c) Unbiased root-mean-square difference (ubRMSD) between Soil Moisture Active Passive soil moisture and Cyclone Global Navigation Satellite System-derived soil moisture. Colored circles are locations shown by the time series in Figure 5.

consistent with the lack of SM variations shown by SMAP, although there is more noise in the record from CYGNSS compared with SMAP. At this site, the absence of substantial variations in SM and noise in the CYGNSS data yield a low correlation ($r = 0.35$).

A map of correlation coefficients for the grid cells used in this study is shown in Figure 4a.

The correlation between $\Delta P_{r,\mathrm{eff}}$ and ΔSM exceeds 0.7 in many locations and is highest in the wettest regions. In contrast, the correlation coefficient is low ($r < 0.2$) in many arid regions. In these areas, there is limited variability in SM throughout the period of record; a low correlation is expected given noise in the CYGNSS and SMAP data. This is consistent with the example data displayed in Figure 3c. A low correlation between $\Delta P_{r,\mathrm{eff}}$ and ΔSM does not indicate that CYGNSS data have limited value for SM detection in arid regions, as discussed below.

The sensitivity of $P_{r,\mathrm{eff}}$ to changes in SM varies spatially (Figure 4b). First, we consider areas where the correlation between $\Delta P_{r,\mathrm{eff}}$ and ΔSM is high ($r > 0.6$), generally corresponding to the wetter areas of the tropics. In these areas, the sensitivity varies from 0.025 to 0.055 $\mathrm{cm^3 \cdot cm^{-3} \cdot dB^{-1}}$, as shown in the examples in Figures 3d and 3e. Conversely, the slope of the linear regression between $\Delta P_{r,\mathrm{eff}}$ and ΔSM is close to 0 in the most arid regions, corresponding to the areas with the lowest correlation between $\Delta P_{r,\mathrm{eff}}$ and ΔSM (e.g., Figure 3f). This is an artifact of the limited SM fluctuations that occur in these areas. Figure 4b shows hatch marks in the areas where the calculated slope/sensitivity is likely not representative of the true sensitivity.

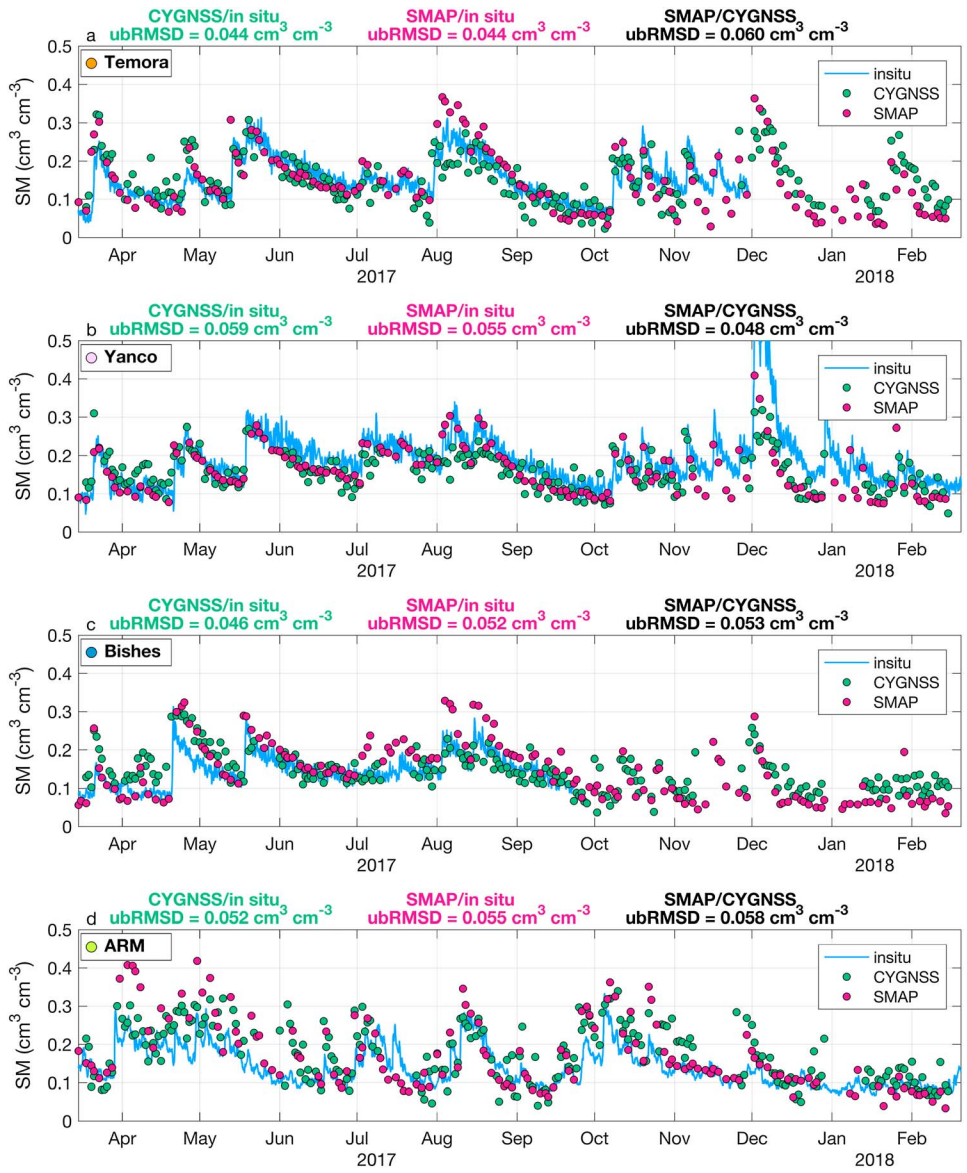

Figure 5. In situ soil moisture observations from four COSMOS sites (indicated by the colored dots shown on the map in Figure 4c), Soil Moisture Active Passive (SMAP) soil moisture (SM) retrievals, and Cyclone Global Navigation Satellite System (CYGNSS)-derived SM for the same locations. ubRMSD = unbiased root-mean-square difference.

4. Estimating SM Fluctuations From CYGNSS

The correlation between $\Delta P_{r,\mathrm{eff}}$ and ΔSM demonstrates CYGNSS is sensitive to both spatial (Figure 2) and temporal (Figure 3) variations in SM. However, the correlation alone does not allow for a complete evaluation of CYGNSS. In areas with minimal SM fluctuations, a low correlation is expected given typical sensor noise (e.g., Colliander et al., 2017). Comparisons of satellite-based observations with in situ SM, modeled data, or SM products from other sensors are typically summarized in terms of unbiased root-mean-square difference (ubRMSD), which requires conversion to standard SM units. We converted CYGNSS $\Delta P_{r,\mathrm{eff}}$ to corresponding SM values using the pixel-by-pixel sensitivities derived via linear regression with SMAP (Figure 4b). We utilized the mean SMAP SM value from each grid cell to reference the CYGNSS-based SM to an absolute scale. Because CYGNSS is referenced to SMAP via the mean values of each, comparisons are inherently unbiased.

The overall ubRMSD between SMAP and CYGNSS is 0.045 cm^3/cm^3, using data from all SMAP pixels with both $\Delta P_{r,\mathrm{eff}}$ and ΔSM observations. This value of ubRMSD is lower than that typically found when SMAP SM is

compared to data from other space-based sensors (e.g., Burgin et al., 2017). This indicates that GNSS reflections measured by CYGNSS could be used to provide useful SM data, preferably using a retrieval algorithm that is independent of SMAP. The ubRMSD between SMAP and CYGNSS varies spatially, from close to 0.0 to more than 0.10 cm^3/cm^3 (Figure 4c). The ubRMSD tends to be lowest in arid regions. Even with noise in the CYGNSS observations (e.g., Figure 3c), CYGNSS $\Delta P_{r,\mathrm{eff}}$ reliably documents little or no variations in SM in these arid locations. The ubRMSD is highest in the Sahel and eastern India, possibly due to land surface heterogeneity at scales finer than SMAP pixels, insufficient open water masking, or incoherent scattering due to vegetation. All of these factors would increase the amount of noise in the CYGNSS observations in these areas, leading to high ubRMSD.

SM estimated from CYGNSS also compares favorably to in situ SM observations from four COSMOS (Cosmic-ray Soil Moisture Observing System) sites in the tropics (Figure 5), data that have been used in previous satellite validation studies (Chan et al., 2018; Montzka et al., 2017). The CYGNSS-based estimates clearly track the SM fluctuations determined from COSMOS: ubRMSD between CYGNSS and COSMOS is between 0.04 and 0.06 cm^3/cm^3. This is similar, and in two of the four cases better than, the ubRMSD between the SMAP and COSMOS records. Knowledge of the sensitivity of $\Delta P_{r,\mathrm{eff}}$ to changes in SM is required for a comparison to in situ observations, which in this case was determined from the intercomparison with SMAP.

An independent retrieval algorithm to produce a CYGNSS-derived SM product would not rely fully on another satellite data product to determine the sensitivity to SM fluctuations, as we have done here. The development of mature electrodynamic models, alongside further analysis of in situ data, will provide more complete insight into how $P_{r,\mathrm{eff}}$ can be used to retrieve SM. However, the procedure used here does provide one benefit—by directly linking $P_{r,\mathrm{eff}}$ to SMAP data, one effectively calibrates the CYGNSS signal to SMAP SM. This would allow the use of CYGNSS data to infill between successive SMAP overpasses, which occur every 2–3 days.

Although the CYGNSS constellation was not designed to sense near-surface SM, the forward scattered L-band signals it records shows strong sensitivity to SM. There are consistent linear relationships between CYGNSS observations and SMAP SM retrievals, which are most easily quantified in areas where the range of SM is highest. This finding supports the idea that spaceborne GNSS-R could provide a complementary approach to traditional approaches of satellite remote sensing of SM.

Acknowledgments
The authors declare no conflict of interests. CYGNSS data can be publicly downloaded from the NASA PO.DAAC. COSMOS soil moisture can be downloaded from http://cosmos.hwr.arizona.edu/.

References

Brocca, L., Hasenauer, S., Lacava, T., Melone, F., Moramarco, T., Wagner, W., et al. (2011). Soil moisture estimation through ASCAT and AMSR-E sensors: An intercomparison and validation study across Europe. *Remote Sensing of Environment*, *115*(12), 3390–3408. https://doi.org/10.1016/j.rse.2011.08.003

Burgin, M. S., Colliander, A., Njoku, E. G., Chan, S. K., Cabot, F., Kerr, Y. H., et al. (2017). A comparative study of the SMAP passive soil moisture product with existing satellite-based soil moisture products. *IEEE Transactions on Geoscience and Remote Sensing*, *55*(5), 2959–2971. https://doi.org/10.1109/TGRS.2017.2656859

Camps, A., Park, H., Pablos, M., Foti, G., & Gommenginger, C. P. (2016). Sensitivity of GNSS-R spaceborne observations to soil moisture and vegetation. *IEEE Journal of Selected Topics in Applied Earth Observations and Remote Sensing*, *9*(10), 4730–4742.

Cardellach, E., Fabra, F., Nogués-Correig, O., Oliveras, S., Ribó, S., & Rius, A. (2011). GNSS-R ground-based and airborne campaigns for ocean, land, ice, and snow techniques: Application to the GOLD-RTR data sets. *Radio Science*, *46*, RS0C04. https://doi.org/10.1029/2011RS004683

Chan, S. K., Bindlish, R., O'Neill, P., Jackson, T., Njoku, E., Dunbar, S., et al. (2018). Development and assessment of the SMAP enhanced passive soil moisture product. *Remote Sensing of Environment*, *204*, 931–941. https://doi.org/10.1016/j.rse.2017.08.025

Chew, C., Shah, R., Zuffada, C., Hajj, G., Masters, D., & Mannucci, A. J. (2016). Demonstrating soil moisture remote sensing with observations from the UK TechDemoSat-1 satellite mission. *Geophysical Research Letters*, *43*, 3317–3324. https://doi.org/10.1002/2016GL068189

Clarizia, M. P., Gommenginger, C. P., Gleason, S. T., Srokosz, M. A., Galdi, C., & Di Bisceglie, M. (2009). Analysis of GNSS-R delay-Doppler maps from the UK-DMC satellite over the ocean. *Geophysical Research Letters*, *36*, L02608. https://doi.org/10.1029/2008GL036292

Colliander, A., Jackson, T. J., Bindlish, R., Chan, S., Das, N., Kim, S. B., et al. (2017). Validation of SMAP surface soil moisture products with core validation sites. *Remote Sensing of Environment*, *191*, 215–231. https://doi.org/10.1016/j.rse.2017.01.021

De Roo, R. D., Du, Y., Ulaby, F. T., & Craig Dobson, M. (2001). A semi-empirical backscattering model at L-band and C-band for a soybean canopy with soil moisture inversion. *IEEE Transactions on Geoscience and Remote Sensing*, *39*(4), 864–872. https://doi.org/10.1109/36.917912

De Roo, R. D., & Ulaby, F. T. (1994). Bistatic specular scattering from rough dielectric surfaces. *IEEE Transactions on Antennas and Propagation*, *42*(2), 220–231. https://doi.org/10.1109/8.277216

Dobson, M. C., Ulaby, F. T., Hallikainen, M. T., & El-Rayes, M. A. (1985). Microwave dielectric behavior of wet soil—Part II: Dielectric mixing models. *IEEE Transactions on Geoscience and Remote Sensing*, *GE-23*(1), 35–46. https://doi.org/10.1109/TGRS.1985.289498

Draper, C. S., Reichle, R. H., De Lannoy, G. J. M., & Liu, Q. (2012). Assimilation of passive and active microwave soil moisture retrievals. *Geophysical Research Letters*, *39*, L04401. https://doi.org/10.1029/2011GL050655

Egido, A. (2013). GNSS reflectometry for land remote sensing applications, PhD Thesis. Retrieved from http://tdx.cat/handle/10803/129090

Egido, A., Paloscia, S., Motte, E., Guerriero, L., Pierdicca, N., Caparrini, M., et al. (2014). Airborne GNSS-R polarimetric measurements for soil moisture and above-ground biomass estimation. *IEEE Journal of Selected Topics in Applied Earth Observations and Remote Sensing*, *7*(5), 1522–1532. https://doi.org/10.1109/JSTARS.2014.2322854

Entekhabi, D., Njoku, E. G., Neill, P. E. O., Kellogg, K. H., Crow, W. T., Edelstein, W. N., et al. (2010). The Soil Moisture Active Passive (SMAP) mission. *Proceedings of the IEEE*, *98*(5), 704–716.

Entekhabi, D., Rodriguez-Iturbe, I., & Castelli, F. (1996). Mutual interaction of soil moisture state and atmospheric processes. *Journal of Hydrology*, *184*(1–2), 3–17.

Ferrazzoli, P., Guerriero, L., Pierdicca, N., & Rahmoune, R. (2011). Forest biomass monitoring with GNSS-R: Theoretical simulations. *Advances in Space Research*, *47*(10), 1823–1832. https://doi.org/10.1016/j.asr.2010.04.025

Foti, G., Gommenginger, C., Jales, P., Unwin, M., Shaw, A., Robertson, C., & Rosellõ, J. (2015). Spaceborne GNSS reflectometry for ocean winds: First results from the UK TechDemoSat-1 mission. *Geophysical Research Letters*, *42*, 5435–5441. https://doi.org/10.1002/2015GL064204

Geudtner, D., & Torres, R. (2012). Sentinel-1 system overview and performance. In *2012 IEEE International Geoscience and Remote Sensing Symposium, Munich* (pp. 1719–1721). https://doi.org/10.1109/IGARSS.2012.6351191

Guerriero, L., Pierdicca, N., Egido, A., Caparrini, M., Paloscia, S., Santi, E., & Floury, N. (2013). Modeling of the GNSS-R signal as a function of soil moisture and vegetation biomass. In *2013 IEEE International Geoscience and Remote Sensing Symposium, Melbourne* (pp. 4050–4053). https://doi.org/10.1109/IGARSS.2013.6723722

Katzberg, S. J., & Garrison, J. L. (1996). Utilizing GPS to determine ionospheric delay over the ocean. *Nasa Technical Memorandum TM-4750*, 1–16. 10.1.1.31.3748

Katzberg, S. J., Torres, O., Grant, M. S., & Masters, D. (2006). Utilizing calibrated GPS reflected signals to estimate soil reflectivity and dielectric constant: Results from SMEX02. *Remote Sensing of Environment*, *100*(1), 17–28. https://doi.org/10.1016/j.rse.2005.09.015

Kerr, Y. H., Waldteufel, P., Richaume, P., Wigneron, J. P., Ferrazzoli, P., Mahmoodi, A., et al. (2012). The SMOS soil moisture retrieval algorithm. *IEEE Transactions of Geoscience and Remote Sensing*, *50*, 1384–1403.

Komjathy, A., Zavorotny, V. U., Axelrad, P., Born, G. H., & Garrison, J. L. (2000). GPS signal scattering from sea surface. *Remote Sensing of Environment*, *73*(2), 162–174. https://doi.org/10.1016/S0034-4257(00)00091-2

Koster, R. D., Dirmeyer, P. A., Guo, Z., Bonan, G., Chan, E., Cox, P., et al. (2004). Regions of strong coupling between soil moisture and precipitation. *Science*, *305*(5687), 1138–1140. https://doi.org/10.1126/science.1100217

Larson, K. M., Small, E. E., Gutmann, E. D., Bilich, A. L., Braun, J. J., & Zavorotny, V. U. (2008). Use of GPS receivers as a soil moisture network for water cycle studies. *Geophysical Research Letters*, *35*, L24405. https://doi.org/10.1029/2008GL036013

Lievens, H., Reichle, R. H., Liu, Q., De Lannoy, G. J. M., Dunbar, R. S., Kim, S. B., et al. (2017). Joint Sentinel-1 and SMAP data assimilation to improve soil moisture estimates. *Geophysical Research Letters*, *44*, 6145–6153. https://doi.org/10.1002/2017GL073904

Masters, D., Zavorotny, V., Katzberg, S., & Emery, W. (2000). GPS signal scattering from land for moisture content determination. *IGARSS 2000*. IEEE 2000 International Geoscience and Remote Sensing Symposium. Taking the Pulse of the Planet: The Role of Remote Sensing in Managing the Environment. *Proceedings (Cat. No.00CH37120)*, *7*, 3090–3092. https://doi.org/10.1109/IGARSS.2000.860346

Masters, D. S. (2004). Surface remote sensing applications of GNSS bistatic radar: Soil moisture and aircraft altimetry. ProQuest Dissertations and Theses, 3153856, 224–224. Retrieved from http://ezproxy.net.ucf.edu/login?url=http://search.proquest.com/docview/305203577?accountid=10003%5Cnhttp://sfx.fcla.edu/ucf?url_ver=Z39.88-2004%rft_val_fmt=info:ofi/fmt:kev:mtx:dissertation%genre=dissertations+%+theses%sid=ProQ:ProQuest+Dissertations+%+The

Montzka, C., Bogena, H. R., Zreda, M., Monerris, A., Morrison, R., Muddu, S., & Vereecken, H. (2017). Validation of spaceborne and modelled surface soil moisture products with cosmic-ray neturon probes. *Remote Sensing*, *9*(2), 1–30.

Naeimi, V., Scipal, K., Bartalis, Z., Hasenauer, S., & Wagner, W. (2009). An improved soil moisture retrieval algorithm for ERS and METOP scatterometer observations. *IEEE Transactions of Geoscience and Remote Sensing*, *47*(7), 1999–2013.

Nghiem, S. V., Zuffada, C., Shah, R., Chew, C., Lowe, S. T., Mannucci, A. J., et al. (2017). Wetland monitoring with Global Navigation Satellite System reflectometry. *Earth and Space Science*, *4*(1), 16–39.

O'Neill, P. E., Chan, S., Njoku, E. G., Jackson, T., & Bindlish, R. (2016). *SMAP enhanced L3 radiometer global daily 9 km EASE-grid soil moisture, version 1*. Boulder, CO: NASA National Snow and Ice Data Center Distributed Active Archive Center. https://doi.org/10.5067/ZRO7EXJ8O3XI

Pierdicca, N., Guerriero, L., Giusto, R., Brogioni, M., & Egido, A. (2014). SAVERS: A simulator of GNSS reflections from bare and vegetated soils. *IEEE Transactions on Geoscience and Remote Sensing*, *52*(10), 6542–6554. https://doi.org/10.1109/TGRS.2013.2297572

Reichle, R., De Lannoy, G., Koster, R. D., Crow, W. T., & Kimball, J. S. (2017). *SMAP L4 9 km EASE-grid surface and root zone soil moisture geophysical data, Version 3*. Boulder, Colorado USA: NASA National Snow and Ice Data Center Distributed Active Archive Center. https://doi.org/10.5067/B59DT1D5UMB4

Rodriguez-Alvarez, N., Bosch-Lluis, X., Camps, A., Aguasca, A., Vall-Llossera, M., Valencia, E., et al. (2011). Review of crop growth and soil moisture monitoring from a ground-based instrument implementing the Interference Pattern GNSS-R Technique. *Radio Science*, *46*, RS0C03. https://doi.org/10.1029/2011RS004680

Rodriguez-Iturbe, I. (2000). Ecohydrology: A hydrologic perspective of climate-soil-vegetation dynamics. *Water Resources Research*, *36*(1), 3–9.

Rudiger, C., Calvet, J.-C., Gruhier, C., Holmes, T., de Jeu, R., & Wagner, W. (2009). An intercomparison of ERS-Scat and AMSR-E soil moisture observations with model simulations over France. *Journal of Hydrometeorology*, *10*, 431–447.

Ruf, C., Atlas, R., Chang, P., Clarizia, M. P., Garrison, J., Gleason, S., et al. (2016). New ocean winds satellite mission to probe hurricanes and tropical convection. *Bulletin of the American Meteorological Society*, 385–396.

Small, E. E., Larson, K. M., Chew, C. C., Dong, J., & Ochsner, T. E. (2016). Validation of GPS-IR soil moisture retrievals: Comparison of different algorithms to remove vegetation effects. *IEEE Journal of Selected Topics in Applied Earth Observations and Remote Sensing*, *9*(10), 1–12. https://doi.org/10.1109/JSTARS.2015.2504527

Su, C.-H., Ryu, D., Young, R. I., Western, A. W., & Wagner, W. (2013). Inter-comparison of microwave satellite soil moisture retrievals over the Murrumbidgee Basin, southeast Australia. *Remote Sensing of Environment*, *134*, 1–11. https://doi.org/10.1016/j.rse.2013.02.016

Valencia, E., Zavorotny, V. U., Akos, D. M., & Camps, A. (2014). Using DDM asymmetry metrics for wind direction retrieval from GPS ocean-scattered signals in airborne experiments. *IEEE Transactions on Geoscience and Remote Sensing*, *52*(7), 3924–3936. https://doi.org/10.1109/TGRS.2013.2278151